Advanced Model of Acoustic Trim; Effect on NTF Accuracy

Bilen Oytun Peksel

December 2, 2011

Contents

Chapter 1

Introduction

Poroelastic materials are widely used in vehicle industry for noise control purposes. However because of their complex response and frequency dependent nature, these parts are not included in huge finite element models which are built to predict the vibro-acoustic response of the vehicles. These poroelastic layers are usually included as mass distribution giving rather poor results. In order increase NTF prediction accuracy there are some finite element based methods based on the theory which had been developed earlier by M.A Biot. Volvo Car Corporation (VCC) intended to benefit from these methods by including poroelastic material models into their finite element models, using the commercial software CDH/EXEL which was developed by P. Göransson (KTH).

The purpose of this thesis is to implement FEM simulations of poroelastic trim materials into Body-in-Blue models of VCC to increase the prediction accuracy, foresee and overcome possible difficulties during the process and compare it with the measurement data which has been already at hand.

This is an implementation process that has a lot of potential technical problems and difficulties so it has been decided that it would be better if it was done using a simple model of a shoe-box and eliminate those problems and move further into the real car model. Working on a shoe-box model is a safe bet because it has been studied before. This is a simple geometry so the mesh conditions and connections are rather simple and straight forward. Then the next step would be to test more complex mesh conditions on this simple model in order to simulate the potential problems of drawbacks so the complexity of mesh elements and connections are increased step by step.

Finally the trim materials meshed properly and prepared to be integrated into body-in-blue model of Volvo S80. This had been a rather challenging process especially when it comes to couple the trim, the body and the cavity. It seems that there are quite much work to be done in order to incorporate these techniques into daily routine in NVH departments. After overcoming the problems faced the simulation results were compared with the measurement data.

Chapter 2

Theoretical Background

Biot's equations which are derived by M.A Biot in 1956 governs this propagation inside porous media. This chapter will only be dealing with the theoretical background of the topic.

Two separate fields are assumed to be present throughout all media which are $u^s$and u^fdisplacements of the frame and pore volume respectively. According to Biot 1956 "There remains however an upper bound for the frequency, namely that at which the wavelength becomes of the order of the pore size". At this frequency the spatial variation of solid frame and fluid particle displacements are too rapid for the homogenized modelling approach embedded to be valid. Also the material under consideration assumed to be isotropic. Following the formulation in [Allard and Atalla, 2009] the wave equations in vector form is given by

$$\begin{aligned} -\omega^2 u^s(\rho_1 - \rho_{12}) - \omega^2 \rho_{12} u^f = (P-N)\nabla\nabla\cdot\mathbf{u}^s + Q\nabla\nabla\cdot\mathbf{u}^f + N\nabla^2\mathbf{u}^s \\ -j\omega\sigma\phi^2 G(\omega)(u^s - u^f) \end{aligned} \tag{2.1}$$

$$-\omega^2 u^f(\phi\rho_0 - \rho_{12}) - \omega^2\rho_{12}u^s = R\nabla\nabla\cdot\mathbf{u}^f + Q\nabla\nabla\cdot\mathbf{u}^s + j\omega\sigma\phi^2 G(\omega)(u^s - u^f) \tag{2.2}$$

where:

For the bulk moduli K_b, K_s, K and the density parameters $\rho_{11}, \rho_{12}, \rho_{22}$ additional discussions needed.

N	The shear modulus of the frame
$R = \frac{\phi^2 K_s}{1-\phi-K_b+\phi K_s/K}$	Homogeneous fluid compressibility stiffness
$Q = \frac{\left[1-\phi-K_b/K_s\right]\phi K_s}{1-\phi-K_b/K_s+\phi K_s/K}$	The potential coupling coefficient
$P = \frac{(1-\phi)\left[1-\phi-\frac{K_b}{K_s}\right]K_s+\phi\frac{K_s}{K}K_b}{1-\phi-K_b/K_s+\phi K_s/K_b} + \frac{4}{3}N$	
ϕ	Porosity: the ratio of volume of t he fluid to total volume.
σ	Flow resistivity
ω	Angular frequency
u^f	The macroscopic average displacement vectors for fluid
u^s	The displacement vectors for frame
$G(\omega)$	The frequency dependent function of visco-inertial drag.

Table 2.1: Parameters and Their Definitions

2.1 Bulk Moduli

The bulk moduli discussed above can be explained using two of three "Gedanken Experiments" discussed by [Biot and Willis, 1957] by first introducing the stress-strain relations in the Biot theory.

$$\sigma_{ij}^s = [(P - 2N)\theta^s + Q\theta^f]\delta_{ij} + 2Ne_{ij}^s \tag{2.3}$$

$$\sigma_{ij}^f = (-\phi p)\delta_{ij} = (Q\theta^s + R\theta^f)\delta_{ij} \tag{2.4}$$

where σ_{ij} and e_{ij} are stress and strain tensors;θ^f and θ^s are the dilatations of the fluid and the solid respectively and defined as:

$$\begin{aligned} \theta^s &= \nabla \cdot u^s \\ \theta^f &= \nabla \cdot u^f \end{aligned}$$

The second Gedanken experiment suggests that the sample shall be surrounded by a flexible jacket which is subjected to a pressure p_1 while the pressure inside is kept at constant p_0 with a pipe. In this test entire pressure applied (p_1) is transmitted to the solid portions of the surface but the pressure of fluid inside the pore remains constant.

This means the that solid dilatation would only be due to the pressure p_1 applied which means:

$$K_b = -p_1/\theta_1^s \tag{2.5}$$

This bulk modulus can be considered as the property of the sole frame in vacuum.

In the third Gedanken experiment the sample is non-jacketed and subjected to a pressure of p_2 while this pressure penetrates into the pores, thus into the fluid inside completely. The bulk modulus in this case called K_s and given by:

$$K_s = -p_2/\theta_2^s \tag{2.6}$$

and the fluid bulk density is given by:

$$K_f = -p_2/\theta_2^f \tag{2.7}$$

In order to complete the discussion on bulk moduli the frequency dependent bulk modulus K needs to be introduced. Although several models exist one of them will be discussed in this thesis.

2.1.1 Champoux-Allard Model for Bulk Modulus

According to this model [Champoux and Allard, 2009] the bulk modulus given at high frequencies to first order approximation in $1/\sqrt{\omega}$

$$K = \frac{\gamma P_0}{\gamma - (\gamma - 1)\left[1 - (1 - j)\frac{\delta}{\Lambda' B}\right]}$$

where$P_0$is ambient mean pressure, B^2 is the Prandtl number, c_p& c_v are specific heats under constant pressure and temperature thus $\gamma = c_p/c_v$.

Λ' is defined as thermal characteristic length given by:

$$\frac{2}{\Lambda'} = \frac{\int_A dA}{\int_V dV} = \frac{A}{S}$$

where the nominator integral is evaluated over surfaces A, while the denominator integral is evaluated over the volume V of the pore.

2.2 Density Parameters:Inertial Forces in the Biot Theory

Since the porous frame assumed to be saturated by a non-viscous fluid, the velocity in the medium could be denoted by $\dot{u}$ and the density by ρ_0 and the components of the inertial force per unit volume can be written as:

$$F_i = \frac{\partial}{\partial t}\frac{\partial E_c}{\partial \dot{u}_i} \tag{2.8}$$

However the kinetic energy would not be generalized as expected as:

$$\frac{1}{2}\rho_1|\dot{u}^s|^2 + \frac{1}{2}\rho_0|\dot{u}^f|^2 \tag{2.9}$$

This is because $\dot{u}^f$ is not the true velocity of the fluid but it is the macroscopic velocity, so kinetic energy in Biot theory for this case would be:

$$E_c = \frac{1}{2}\rho_{11}|\dot{u}^s|^2 + \rho_{12}\dot{u}^s\dot{u}^f + \frac{1}{2}\rho_{22}|\dot{u}^f|^2 \tag{2.10}$$

$\rho_{11}, \rho_{12}, \rho_{22}$ are related to the geometry of the frame and do not depend on the frequency. The components of inertial forces acting on the frame and on the air respectively

$$q_i^s = \frac{\partial}{\partial t}\frac{\partial E_c}{\partial \dot{u}_i^s} = \rho_{11}\ddot{u}_i^s + \rho_{12}\ddot{u}_i^f \tag{2.11}$$

$$q_i^f = \frac{\partial}{\partial t}\frac{\partial E_c}{\partial \dot{u}_i^f} = \rho_{12}\ddot{u}_i^s + \rho_{22}\ddot{u}_i^f \tag{2.12}$$

If the case that fluid and frame move in phase together with the same velocity is considered:

$$\dot{u}^s = \dot{u}^f \tag{2.13}$$

then (2.9) would be valid and could be rewritten as:

$$E_c = \frac{1}{2}(\rho_1 + \phi\rho_0)|\dot{u}^s|^2 \tag{2.14}$$

If one compares (2.14) and (2.10) the relation between densities can be written as:

$$\rho_{11} + 2\rho_{12} + \rho_{22} = \rho_1 + \phi\rho_0 \tag{2.15}$$

The components q_i^f of the inertial force per unit volume of material are given by:

$$q_i^f = \phi\rho_0\frac{\partial^2 u_i^f}{\partial t^2} \tag{2.16}$$

Comparing (2.16) and (2.12) following relations are obtained:

$$\phi\rho_0 = \rho_{22} + \rho_{12} \tag{2.17}$$

$$\rho_1 = \rho_{11} + \rho_{12} \tag{2.18}$$

where the coefficient ρ_{12} represents a mass coupling parameter between fluid and solid.
If the frame assumed to be constrained and not moving (2.12) becomes:

$$q_i^f = \rho_{22}\ddot{u}_i^f$$

and this is the inertial force acting on non viscous fluid, yet the following equation can be written:

$$\rho_{22}\ddot{u}^f = \alpha_\infty \phi \rho_0 \ddot{u}^f \tag{2.19}$$

where α_∞ being the classical tortuosity described in [Johnson et al., 1987] simply can be related to effective densities by:

$$\rho = \alpha_\infty \rho_0 \tag{2.20}$$

From (2.17) and (2.19) :

$$\rho_{12} = -\phi\rho_0(\alpha_\infty - 1) \tag{2.21}$$

For a viscous fluid the effective density shall be estimated using dynamic tortuosity. There are several estimations. In this thesis one of them, Johnson model will be discussed.

2.2.1 Johnson Model of Dynamic Tortuosity

The dynamic tortuosity is defined in [Johnson et al., 1987] as

$$\alpha(\omega) = \frac{\nu\phi}{jwq_0}\left\{1 + \left[1 + \left(\frac{2\alpha_\infty q_0}{b\phi\Lambda}\right)^2 \frac{j\omega}{\nu}\right]^{1/2}\right\} + \alpha_\infty$$

where $q_0$is the static viscous permeability, $\nu = \eta/\rho_0$ namely the viscosity-density ratio.
An expression to be used in wave equations can be extracted:

$$G_j(\omega) = \left[1 + \left(\frac{2\alpha_\infty q_0}{\phi\Lambda}\right)^2 \frac{j\omega}{\nu}\right]^{1/2}$$

This frequency dependent function $G(\omega)$ describes the viscous drag and is completely determined by the micro structure.
Ais the viscous characteristic length and the given by [Johnson et al., 1986]

$$\frac{2}{\Lambda} = \frac{\int_A v_i^2(r_w)dA}{\int_V v_i^2(r)dV}$$

where $v_i(r_w)$ is the velocity of the fluid on the pore surface and the integral is evaluated over surfaces A, while $v_i(r)$ is the velocity inside the pores and the integral is evaluated over the volume V of the pore.

2.3 Building Wave Equations

The equations of motion in an elastic solid without external forces can be written as:

$$\rho\frac{\partial^2 u_i^s}{\partial t^2} = (K_c - \mu)\frac{\partial\theta^s}{\partial x_i} + \mu\nabla^2 u_i^s \tag{2.22}$$

where μ is one of the lame coefficients.
For the non viscous fluid case LHS of (2.22) is given by (2.11) where $\rho_{11} = \rho_1 - \rho_{12}$

$$\rho\frac{\partial^2 u_i^s}{\partial t^2} \rightarrow (\rho_1 - \rho_{12})\frac{\partial^2 u_i^s}{\partial t^2} + \rho_{12}\frac{\partial^2 u_i^f}{\partial t^2} \qquad i = 1,2,3 \tag{2.23}$$

For a viscous fluid α_∞ in ρ_{12} is replaced by $\alpha_\infty + \frac{\nu\phi}{j\omega q_o}G(\omega)$. Finally when this term is inserted into inertial coupling term $\omega^2\rho_{12}(u_i^s - u_i^f)$; $K_c - \mu$ and μ are replaced by P and N respectively (2.1) & (2.2) are obtained. By this addition, a coupling due to viscosity of fluid namely viscous forces between the fluid and the frame which is generated by a relative velocity between fluid and the frame.

Another formalism for density parameters is to include visco-inertial drag into density parameters.

$$\tilde{\rho}_{11} = \rho_1 - \rho_{12} - j\sigma\phi^2\frac{G(\omega)}{\omega} \tag{2.24}$$

$$\tilde{\rho}_{12} = \rho_{12} + j\sigma\phi^2\frac{G(\omega)}{\omega} \tag{2.25}$$

$$\tilde{\rho}_{22} = \phi\rho_0 - \rho_{12} - j\sigma\phi^2\frac{G(\omega)}{\omega} \tag{2.26}$$

So Biot vector form equations could be written as:

$$-\omega^2(\tilde{\rho}_{11}\boldsymbol{u}^s + \tilde{\rho}_{12}\boldsymbol{u}^f) = (P-N)\boldsymbol{\nabla}\boldsymbol{\nabla}\cdot\boldsymbol{u}^s + N\boldsymbol{\nabla}^2\boldsymbol{u}^s + Q\boldsymbol{\nabla}\boldsymbol{\nabla}\cdot\boldsymbol{u}^f \tag{2.27}$$

$$-\omega^2(\tilde{\rho}_{22}\boldsymbol{u}^f + \tilde{\rho}_{12}\boldsymbol{u}^s) = R\boldsymbol{\nabla}\boldsymbol{\nabla}\cdot\boldsymbol{u}^f + Q\boldsymbol{\nabla}\boldsymbol{\nabla}\cdot\boldsymbol{u}^s \tag{2.28}$$

2.4 Acoustic Simplification

Almost all of the materials that used for acoustic purposes have frame stiffness much larger than air. Those frame materials are not compressible yet when saturated with air they are sound absorbing. A unit volume of material contains a volume $(1-\phi)$ of frame at $p=0$. When this structure is compressed namely a pressure different from zero is applied, the same volume of frame is in a volume of porous material equal to $1+\theta^s$ and the porosity is given by:

$$1-\phi = (1-\phi')(1+\theta^s) \tag{2.29}$$

θ^f: the dilation of air in the material due to variation of porosity is given by:

$$\phi'(1+\theta^f) = \phi \tag{2.30}$$

Equating (2.29)&(2.30):

$$\theta^f = \frac{(1-\phi)}{\phi}\theta^s \tag{2.31}$$

So by this simplification P,Q and R can rewritten as:

- $R = \phi K$
- $Q = K(1-\phi)$
- $P = \frac{4}{3}N + K_b + \frac{(1-\phi)^2}{\phi}K$

Since all the materials used in this project are as such above simplification will be used for the rest of the work.

2.5 Separation of Variables: Two Compressional Waves and the Shear Wave

The separation of the wave equations in terms of compressional and shear waves can be done by defining displacement scalar potentials for those waves.

2.5.1 Compressional Waves

Defining vector potentials for both fluid and solid

$$u^s = \nabla\varphi^s \tag{2.32}$$

$$u^f = \nabla\varphi^f \tag{2.33}$$

By using (2.27)&(2.28) the following relation can be written:

$$-\omega^2(\tilde{\rho}_{11}\varphi^s + \tilde{\rho}_{12}\varphi^f) = P\nabla^2\varphi^s + Q\nabla^2\varphi^f \tag{2.34}$$

$$-\omega^2(\tilde{\rho}_{22}\varphi^f + \tilde{\rho}_{12}\varphi^s) = R\nabla^2\varphi^f + Q\nabla^2\varphi^s \tag{2.35}$$

If,

$$[\varphi] = \left[\varphi^s, \varphi^f\right]^T \tag{2.36}$$

then (2.34)&(2.35) can be written as

$$-\omega^2[\rho][\varphi] = [M]\nabla^2[\varphi] \tag{2.37}$$

where

$$[\rho] = \begin{bmatrix} \tilde{\rho}_{11} & \tilde{\rho}_{12} \\ \tilde{\rho}_{12} & \tilde{\rho}_{22} \end{bmatrix}, \quad [M] = \begin{bmatrix} P & Q \\ Q & R \end{bmatrix} \tag{2.38}$$

So (2.34)&(2.35) can be written as

$$-\omega^2[M]^{-1}[\rho][\varphi] = \nabla^2[\varphi] \tag{2.39}$$

Let δ_1^2 and δ_2^2 be the eigenvalues and $[\varphi_1]$ and $[\varphi_2]$ be the eigenvector solutions of the equation system then those quantities relate as:

$$-\delta_1^2[\varphi_1] = \nabla^2[\varphi_1] \tag{2.40}$$

$$-\delta_2^2[\varphi_2] = \nabla^2[\varphi_2] \tag{2.41}$$

so δ_1^2 and δ_2^2 are given by:

$$\delta_1^2 = \frac{\omega^2}{2(PR-Q^2)}[P\tilde{\rho}_{22} + R\tilde{\rho}_{11} - 2Q\tilde{\rho}_{12} - \sqrt{\Delta} \tag{2.42}$$

$$\delta_2^2 = \frac{\omega^2}{2(PR-Q^2)}[P\tilde{\rho}_{22} + R\tilde{\rho}_{11} - 2Q\tilde{\rho}_{12} + \sqrt{\Delta} \tag{2.43}$$

where

$$\Delta = [P\tilde{\rho}_{22} + R\tilde{\rho}_{11} - 2Q\tilde{\rho}_{12}]^2 - 4(PR-Q^2)(\tilde{\rho}_{11}\tilde{\rho}_{22} - \tilde{\rho}_{12}^2) \tag{2.44}$$

Eigenvectors can be written as:

$$[\varphi_1] = \begin{bmatrix} \varphi_1^s \\ \varphi_1^f \end{bmatrix}, \quad [\varphi_2] = \begin{bmatrix} \varphi_2^s \\ \varphi_2^f \end{bmatrix} \tag{2.45}$$

Ratio of velocities between frame and air:

$$\varphi_i^f/\varphi_i^s = \frac{P\delta_i^2 - \omega^2\tilde{\rho}_{11}}{\omega^2\tilde{\rho}_{12} - Q\delta_i^2} \qquad i = 1,2 \tag{2.46}$$

or

$$\varphi_i^f/\varphi_i^s = \frac{Q\delta_i^2 - \omega^2\tilde{\rho}_{12}}{\omega^2\tilde{\rho}_{22} - R\delta_i^2} \qquad i = 1,2 \tag{2.47}$$

2.5.2 The Shear Wave

Define a set of displacement vector potentials ψ^s, ψ^f:

$$u^s = \nabla \wedge \psi^s \tag{2.48}$$

$$u^f = \nabla \wedge \psi^f \tag{2.49}$$

Inserting above relations into (2.27)&(2.28) yields:

$$-\omega^2\tilde{\rho}_{11}\psi^s - \omega^2\tilde{\rho}_{12}\psi^f = N\nabla^2\psi^s \tag{2.50}$$

$$-\omega^2\tilde{\rho}_{12}\psi^s - \omega^2\tilde{\rho}_{12}\psi^f = 0 \tag{2.51}$$

Using (2.51) :

$$\psi^f/\psi^s = -\tilde{\rho}_{12}/\tilde{\rho}_{22} \tag{2.52}$$

inserting it into (2.50) the propagation of shear wave inside the frame is given by:

$$\nabla^2\psi^s + \frac{\omega^2}{N}\left(\frac{\tilde{\rho}_{11}\tilde{\rho}_{22} - \tilde{\rho}_{12}^2}{\tilde{\rho}_{22}}\right)\psi^s = 0 \tag{2.53}$$

The eigenvalue is given by:

$$\delta_3^2 = \frac{\omega^2}{N}\left(\frac{\tilde{\rho}_{11}\tilde{\rho}_{22} - \tilde{\rho}_{12}^2}{\tilde{\rho}_{22}}\right) \tag{2.54}$$

and (2.52) is also equivalent to:

$$\psi^f/\psi^s = \frac{N\delta_3^2 - \omega^2\tilde{\rho}_{11}}{\omega^2\tilde{\rho}_{22}} \tag{2.55}$$

2.6 The Mixed Pressure-Displacement Representation $(u-p)$

The commercial software CDH/EXEL which was used for all the calculations in this project uses the u–p representation. This representation comes along with great advantages. Most important of all is that it reduces the computational effort hugely by eliminating immense amount of degree of freedoms from the equation system. Thus this representation shall be discussed and used for FE formulation later on. "$u-p$" means that instead of $u^s - u^f$, displacement u for solid and pressure p for fluid will be used. Assuming porous materials have homogeneous material properties using stress-strain relations on (2.3)&(2.4), (2.27)&(2.28) can be written as:

$$\begin{cases} \omega^2\tilde{\rho}_{11}u^s + \omega^2\tilde{\rho}_{12}u^f + div\,\sigma^s = 0 \\ \omega^2\tilde{\rho}_{22}u^f + \omega^2\tilde{\rho}_{12}u^s - \phi\nabla p = 0 \end{cases} \tag{2.56}$$

To get rid of dependency on fluid displacement, the fluid displacement term in the second eq. of (2.56) is extracted and put into the first one and following expression is obtained:

$$\omega^2\tilde{\rho}u^s + \phi\frac{\tilde{\rho}_{12}}{\tilde{\rho}_{22}}\nabla p + div\,\sigma^s = 0 \tag{2.57}$$

where $\tilde{\rho} = \tilde{\rho}_{11} - \frac{(\tilde{\rho}_{12})^2}{\tilde{\rho}_{22}}$

However fluid displacement dependency is still embedded in $\sigma^s = \sigma^s(\boldsymbol{u}^s, \boldsymbol{u}^f)$. To eliminate it (2.3)&(2.4) used to get:

$$\sigma^s_{ij}(\boldsymbol{u}^s) = \hat{\sigma}^s_{ij}(\boldsymbol{u}^s) - \phi\frac{\tilde{Q}}{\tilde{R}}p\delta_{ij} \tag{2.58}$$

$\tilde{Q}$ and $\tilde{R}$ points out a possible frequency dependency and $\hat{\sigma}^s_{ij}$ is the classical stress-strain relation for an acoustic solid which is given by:

$$\hat{\sigma}^s_{ij}(\boldsymbol{u}^s) = (K_b - \frac{2}{3}N)div\,\boldsymbol{u}^s + 2Ne^s_{ij} \tag{2.59}$$

Inserting (2.58) into first equation of (2.56)

$$div\,\hat{\sigma}^s_{ij}(\boldsymbol{u}^s) + \tilde{\rho}\omega^2\boldsymbol{u}^s + \tilde{\gamma}\nabla p = 0 \tag{2.60}$$

where $\tilde{\gamma} = \phi\left(\frac{\tilde{\rho}_{12}}{\tilde{\rho}_{22}} - \frac{\tilde{Q}}{\tilde{R}}\right)$
Using the simplification in section 2.4 :

$$\tilde{\gamma} = \phi\left(\frac{\tilde{\rho}_{12}}{\tilde{\rho}_{22}} - \frac{1-\phi}{\phi}\right) \tag{2.61}$$

For the fluid, evaluating the divergence to $\boldsymbol{u}^f$:

$$div\,\boldsymbol{u}^f = \frac{\phi}{\omega^2\tilde{\rho}_{22}}\Delta p - \frac{\tilde{\rho}_{12}}{\tilde{\rho}_{22}}div\,\boldsymbol{u}^s \tag{2.62}$$

inserting into (2.56):

$$\Delta p + \frac{\tilde{\rho}_{22}}{\tilde{R}}\omega^2 p + \frac{\tilde{\rho}_{22}}{\phi^2}\tilde{\gamma}\omega^2 div\,\boldsymbol{u}^s = 0 \tag{2.63}$$

2.7 FE formulation of Biot's Equations

A single equation for the weak form of mixed u-p formulation (2.63)&(2.60) is given by:

$$\begin{aligned}\int_\Omega \left[\hat{\sigma}^s_{ij}\delta e^s_{ij} - \omega^2\tilde{\rho}u^s_i\delta u^s_i\right]d\Omega + \int_\Omega\left[\frac{\phi^2}{\tilde{\alpha}\rho_0\omega^2}\frac{\partial p}{\partial x_i}\frac{\partial(\delta p)}{\partial x_i} - \frac{\phi^2}{\tilde{R}}p\delta p\right]d\Omega \\ - \int_\Omega\frac{\phi}{\tilde{\alpha}}\delta\left(\frac{\partial p}{\partial x_i}u^s_i\right)d\Omega - \int_\Omega\phi\left(1+\frac{\tilde{Q}}{\tilde{R}}\right)\delta(pu^s_{i,i})dS \\ - \int_\Gamma\sigma^t_{ij}n_j\delta u^s_i dS - \int_\Gamma\phi(u^f_n - u^s_n)\delta p dS = 0 \quad \forall(\delta u^s_i, \delta p)\end{aligned} \tag{2.64}$$

where $\tilde{\gamma} + \phi(1 + \tilde{Q}/\tilde{R}) = \phi/\tilde{\alpha}$ and $\tilde{\rho}_{22} = \tilde{\alpha}\rho_0$
This form shows that the coupling between fluid and solid is of two natures:

1. Kinetic (Inertial), $\int_\Omega(\phi/\tilde{\alpha})\delta(u^s_i\partial p/\partial x_i)d\Omega$
2. Potential (Elastic), $\int_\Omega\phi\left(1+\tilde{Q}/\tilde{R}\right)\delta(pu^s_{i,i})dS$

2.7.1 Coupling Conditions

There are three types of coupling conditions implemented in this work.

- Poroelastic-elastic
- Poroelastic-acoustic
- Poroelastic-poroelastic

In (2.64) porous medium couples with other media through the following term:

$$I^p = -\int_\Gamma \sigma_{ij}^t n_j \delta u_i^s dS - \int_\Gamma \phi(u_n^f - u_n^s)\delta p dS \tag{2.65}$$

2.7.1.1 Poroelastic-elastic coupling

In order to describe elastic medium displacement vector u^e, volume and boundary Ω^e and Γ^e will be used. The surface integral of virtual work done by external forces applied on the surface of structural domain is given by

$$I^e = -\int_{\Gamma^e} \sigma_{ij}^e n_j \delta u_i^e dS \tag{2.66}$$

where σ_{ij}^e and e_{ij}^e are components of structure stress and strain tensors, n_j are the components of the outward normal vector to the surface and δu_i^e is an arbitrary admissible variation of u_i^e.

When above integral is combined with the weak formulation of poroelastic medium:

$$I^p + I^e = -\int_\Gamma \sigma_{ij}^t n_j \delta u_i^s dS - \int_\Gamma \phi(u_n^f - u_n^s)\delta p dS + \int_\Gamma \sigma_{ij}^e n_j \delta u_i^e dS \tag{2.67}$$

Finally the coupling conditions are given by:

$$\begin{cases} \sigma_{ij}^t n_j = \sigma_{ij}^e n_j \\ u_n^f - u_n^s = 0 \\ u_i^s = u_i^e \end{cases} \tag{2.68}$$

2.7.1.2 Poroelastic-acoustic coupling

In order to describe acoustic medium pressure field p^a, volume and boundary Ω^a and Γ^a will be used. The surface integral of virtual work done by external forces applied on the surface of acoustic domain is given by

$$I^a = -\frac{1}{\rho_0 \omega^2}\int_{\Gamma^a} \frac{\partial p^a}{\partial n}\delta p^a dS \tag{2.69}$$

where $\partial/\partial n$ is normal derivative and δp^a is an arbitrary admissible variation of p^a.

When above integral is combined with the weak formulation of poroelastic medium:

$$I^p + I^a = -\int_\Gamma \sigma_{ij}^t n_j \delta u_i^s dS - \int_\Gamma \phi(u_n^f - u_n^s)\delta p dS + \frac{1}{\rho_0 \omega^2}\int_{\Gamma^a} \frac{\partial p^a}{\partial n}\delta p^a dS \tag{2.70}$$

Finally the coupling conditions are given by:

$$\begin{cases} \sigma_{ij}^t n_j = -p^a n_i \\ \frac{1}{\rho_0 \omega^2}\frac{\partial p^a}{\partial n} = (1-\phi)u_n^s + \phi u_n^f = u_n^s + \phi(u_n^f - u_n^s) \\ p = p^a \end{cases} \tag{2.71}$$

2.7.1.3 Poroelastic-poroelastic coupling

Two poroelastic mediums are coupled to each other by their solid and pore fluid phases. The subscripts 1 and 2 will be used to identify the displacement vectors and pressure fields of each medium.

$$I_1^p + I_2^p = -\int_\Gamma \sigma_{1ij}^t n_j \delta u_{1i}^s dS - \int_\Gamma \phi_1 (u_{1n}^f - u_{1n}^s)\delta p_1 dS + \int_\Gamma \sigma_{2ij}^t n_j \delta u_{2i}^s dS - \int_\Gamma \phi_2 (u_{2n}^f - u_{2n}^s)\delta p_2 dS \tag{2.72}$$

The coupling conditions are given by:

$$\begin{cases} \sigma_{1ij}^t n_j = \sigma_{2ij}^t n_j \\ \phi_1(u_{1n}^f - u_{1n}^s) = \phi_2(u_{2n}^f - u_{2n}^s) \\ u_{1i}^s = u_{2i}^s \\ p_1 = p_2 \end{cases} \tag{2.73}$$

2.8 Numerical Implementation

The discrete form of (2.64) is:

$$\begin{bmatrix} [Z] & -\left[\tilde{C}\right] \\ -[C]^T & [A] \end{bmatrix} \begin{Bmatrix} u^s \\ p \end{Bmatrix} = \begin{Bmatrix} F^s \\ F^f \end{Bmatrix} \tag{2.74}$$

where $\{u\}$ and $\{p\}$ stands for solid and fluid phase global nodal variables. $[Z] = \omega^2 \left[\tilde{M}\right] + \left[\hat{K}\right]$ is the mechanical impedance matrix of the frame with $\left[\tilde{M}\right]$ and $\left[\hat{K}\right]$ being mass and stiffness matrices:

$$\begin{aligned} \int_\Omega \tilde{\rho} u_i^s \delta u_i^s d\Omega &= \langle \delta u^s \rangle \left[\tilde{M}\right] \{u^s\} \\ \int_\Omega \hat{\sigma}_{ij}^s \delta e_{ij}^s d\Omega &= \langle \delta u^s \rangle \left[\hat{K}\right] \{u^s\} \end{aligned} \tag{2.75}$$

$[A] = \left[\tilde{H}\right]/\omega - \left[\tilde{Q}\right]$ is the acoustic admittance matrix of the fluid with $\left[\tilde{H}\right]$ and $\left[\tilde{Q}\right]$ being equivalent kinetic and compression energy matrices for the fluid phase

$$\begin{aligned} \int_{d\Omega} \frac{\phi^2}{\tilde{\rho}_{22}} \frac{\partial p}{\partial x_i} \frac{\partial(\delta p)}{\partial x_i} d\Omega &= \langle \delta p \rangle \left[\tilde{H}\right] \{p\} \\ \int_\Omega \frac{\phi^2}{\tilde{R}} p \delta p d\Omega &= \langle \delta p \rangle \left[\tilde{Q}\right] \{p\} \end{aligned} \tag{2.76}$$

$\left[\tilde{C}\right] = \left[\tilde{C}_1\right] + \left[\tilde{C}_2\right]$ is a volume coupling matrix between the frame and the fluid variables

$$\begin{aligned} \int_\Omega \frac{\phi}{\tilde{\alpha}} \delta \left(\frac{\partial p}{\partial x_i} u_i^s \right) d\Omega &= \langle \delta u^s \rangle \left[\tilde{C}_1\right] \{p\} + \langle \delta p \rangle \left[\tilde{C}_1\right]^T \{u^s\} \\ \int_\Omega \phi \left(1 + \frac{\tilde{Q}}{\tilde{R}} \right) \delta \left(p u_{i,i}^s \right) dS &= \langle \delta u^s \rangle \left[\tilde{C}_2\right] \{p\} + \langle \delta p \rangle \left[\tilde{C}_2\right]^T \{u^s\} \end{aligned} \tag{2.77}$$

$\{F^s\}$ is the surface loading for the frame

$$\int_\Gamma T_i \delta u_i^s dS = \langle \delta u^s \rangle \{F^s\} \tag{2.78}$$

where $T_i = \sigma_{ij}^t n_j$ represent the components on the coordinate axis x_i of the total stress vector. $\{F^f\}$ is the surface kinematic coupling vector for the fluid:

$$\int_{\Gamma} \phi(u_n^f - u_n^s)\delta p dS = \langle \delta p \rangle \left\{ F^f \right\} \tag{2.79}$$

In the above equations, $\{\}$ denotes a vector and $\langle\rangle$ its transpose.

Chapter 3

Simple Box

Integrating the poroelastic trim models into the Body-in-Blue (BIB) FEM calculations turns out to be a complex job to handle. It is easier to implement these models into a imaginary box with a symmetric and simple geometry. This way the preparations and interpretations of the results would be easier. If something would go wrong which is more than likely, it is easier to fix or understand.

The simulations of the real car body is carried out in MSC NASTRAN platform and the poroelastic parts will be handled by CDH/EXEL tool for NASTRAN platform. So this simple box is designed to fit in with the platform's standard procedures parameters. The finite element model example is originally built by Peter Göransson in KTH by using fortran a code without a pre-processor. Then a similar model with the same geometry is built for this project by BETA/ANSA pre-processor which is used daily in VCC. After this, several manipulations on the finite element model was made in order to understand, foresee and overcome possible difficulties that may occur in the BIB implementation. Finally the response results are to be discussed.

3.1 Definition of the Simple Box

The box consists of one layer of thin steel plate, one layer of poroelastic material, one layer of heavy layer and a rather long cavity on top of them.(See Figure 3.1) The base steel plate fastened on all edges meaning the boundary conditions are defined as 0 displacement. There is a point force defined with $1\,N$ amplitude and up to $1000\,Hz$ frequency with $1\,Hz$ steps. The response points are located at the same z axis and in every layer. In poroelastic medium both structural velocity and pressure fields were probed.

The material properties defined in the calculation were taken from actual material data sheets which are used in the real vehicle. Although poroelastic materials are The material data that both NASTRAN and EXEL demands are presented in Table 3.1 and the dimensions for this configuration are $0.4 \times 0.6 \times 1.293$ in meters. The material data belongs to the ones which were used for the actual carpets used in Volvo S80.

Coupling between the different layers are handled by standard connection types in NASTRAN. The details of coupling will be given for each model in the next section since it differs with the mesh compatibility.

The system is excited by a point force on the steel plate and the sensing points are on the same x-y plane and on every layer including the cavity. The force is a unit force with an harmonic excitation up to 1000 Hz.

	Steel	Porous	Heavy Layer
$t(m)$	8.5×10^{-4}	0.04	0.002
$E(N/m^2)$	2.06×10^{11}	1.76×10^5	3.29×10^8
ν	0.3	0.3	0.4
$\rho(kg/m^3)$	7850	52	1890
η	0.01	0.108	0.27
$\rho_0(kg/m^3)$	N/A	1.2	N/A
ϕ	N/A	0.951	N/A
$\sigma(Ns/m^4)$	N/A	1.3×10^4	N/A
τ	N/A	1.7	N/A
$L_m(m)(\Lambda$, see 2.2.1)	N/A	6×10^{-5}	N/A
$L_{mp}(m)(\Lambda'$, see 2.1.1)	N/A	1.4×10^{-4}	N/A

Table 3.1: I^{st}Configuration Material Data(See table 3.2 for legend)

t	Thickness
E	Young's Modulus
ν	Poisson's Ratio
ρ	Mass Density
η	Loss Factor
ρ_0	Ambient Density
ϕ	Porosity
σ	Flow Resistivity
τ	Tortuosity
$L_m(\Lambda)$	Viscous Characteristic Length
$L_{mp}(\Lambda')$	Thermal Characteristic Length

Table 3.2: Legend

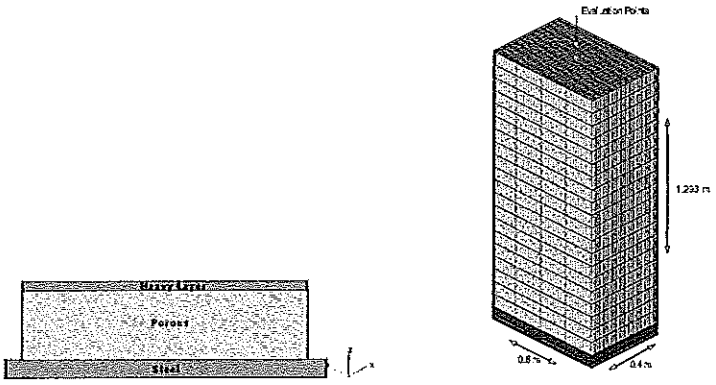

Figure 3.1: Model

3.2 From an Academic Example Towards Industrial

The most basic finite element model prepared as a simple box meshed with solid hexa elements and all coincident nodes. The purpose of this model is to maintain the couplings between different layers in a simple, straight forward fashion. However in the BIB case the elements are usually appear to be tetras and it is almost impossible to find a symmetric coincident nodes between the layers since the geometries of both the trim materials and the structure which they sit upon are largely complex. There is also an additional tools to speed up the eigenvalue solution process by multi-level structuring called AMLS which is heavily depended on in the large BIB calculations. So it would be ensuring to see even after all that changes are made the simple model would run smoothly. Otherwise, it would be beneficial to see what kind of problems may occur before moving on to larger models. Thus this section is mostly about changing this simple shoebox finite element model step by step into a more industrial model. First the different models shall be listed and the results shall be discussed.

Model	Steel Plate	Porous Later	Heavy Layer	Cavity
A	1080 Hexa-Solid	3240 Hexa-Solid	1080 Hexa-Solid	103680 Hexa-Solid
B	1080 Quad-Shell	3240 Hexa-Solid	1080 Hexa-Solid	103680 Hexa-Solid
C	1080 Quad-Shell	2520 Hexa-Solid	1080 Hexa-Solid	103680 Hexa-Solid
D	1080 Quad-Shell	2520 Hexa-Solid	1080 Hexa-Solid	258264 Tetra-Solid
E	1080 Quad-Shell	21369 Tetra-Solid	1080 Hexa-Solid	258264 Tetra-Solid

Table 3.3: Element Types and sizes of Models A-E

Model A As mentioned before this is the most basic academic type model. All the layers created and meshed as solid hexa elements and the meshes are completely compatible with each other. This allows the layers to be coupled easily with node to node coupling. For that NASTRAN's standard RBE2 type connection between steel base and porous material as well as between porous and heavy layer is used (see the yellow nodes in figure 3.2) . For coupling to the cavity NASTRAN's automatic coupling tool ACMODL is used.

Model B In the standard real body models, shell elements are preferred over solid elements for many reasons. So it would be wise to mesh the bottom steel plate as a shell and see the possible effects on the results. Unfortunately the poroelastic parts cannot be modelled with shell elements due to the restrictions of EXEL. The meshes are still compatible so the connections remain same for this model as Model A. "Model B" is basically same model but the bottom steel plate is modeled as a shell and meshed with $27 \times 40 = 1080$ quad elements.

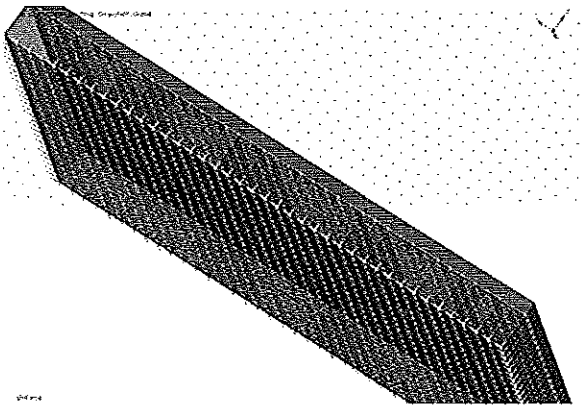

Figure 3.2: Model B

Model C This is the mode model where the connections start to differ. Porous layer mesh in Model B is altered to become incompatible with the neighbouring layers. Now the nodes are not coincident and a different type of coupling must be used. NASTRAN's standard RBE3 connections (see blue lines in Figure 3.3) are used for incompatible coupling instead of RBE2s because the nodes are neither coincident nor same amount namely node to node coupling would not work. An additional specifically designed software called CONNECT provided with CDH/EXEL is used to create these RBE3s. "Model C" is basically same model but the porous mesh is incompatible with the neighbouring material layers. The number of hexa elements for this layer is $24 \times 35 \times 3 = 2520$

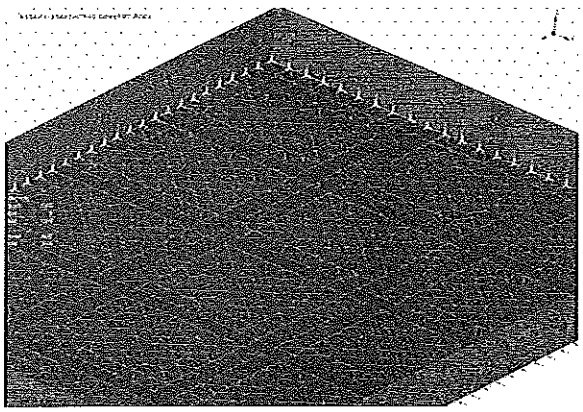

Figure 3.3: Model C

Model D "Model D" is basically same model but the cavity is meshed with tetra solid elements which of course is incompatible with the neighboring heavy layer. The number of hexa elements for this layer is 258264.

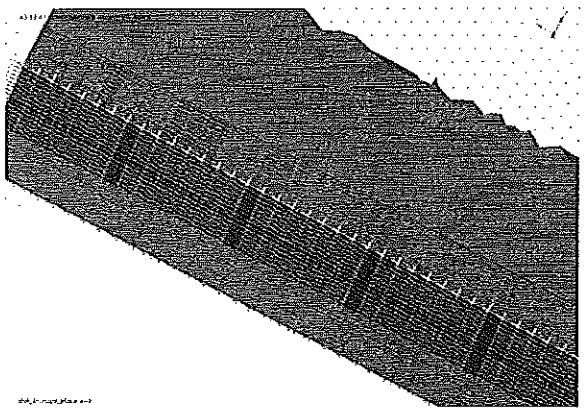

Figure 3.4: Model D

Model E "Model E" which is basically same model but the porous layer is meshed with tetras and of course incompatible with the neighboring layers. The the number of tetra elements for this layer is 21369

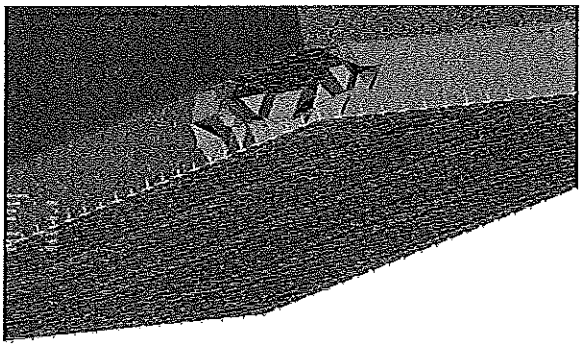

Figure 3.5: Model E

3.3 Results

For every model A-E the results compared with each other in sequence respectively eg. A&B, B&C etc. and finally first model and the last model was compared. The purpose here is to test and catch any possible difference in results for every step and in the end observe the overall difference between the academic and industrial cases.

As stated before 4 different response points have been evaluated and to be analysed. Since the poroelastic layer has actually two different mediums it has two different sub-plots for pressure and velocity field. So 5 different sub-plots listed below in sequence for every case :

1. Cavity Pressure
2. Base Steel Plate Velocity
3. Poroelastic Velocity
4. Heavy Layer Velocity
5. Poroelastic Pressure

The comparison in Figure 3.6 compares the effect of using shell elements instead of solid elements for the base structure which in this case is the thin steel plate. Relatively significant differences are observed in all layers except cavity. In the plate response sub-plot a slight shift can be observed. This shift may be explained by the fact that different differential equations used to define shell and solid type elements. In addition the behaviours of solid and shell elements in terms of degree of freedoms are different. The shell element nodes have 6 dofs the last 3 being rotations. However solid element nodes only have first 3 and the rotations and bending can be defined by multi points creating geometries which an twist and turn.

The shift along the frequency scale cannot be observed in the other comparisons until the comparison between models A&E. However slight differences especially in high frequency range can be observed (see Figures 3.7, 3.8, 3.9). This is rather comprehensible since the coupling mechanisms are affected by the type of connections between the nodes. All the changes during the process can be observed in Figure 3.10. The effect of AMLS is almost non-existent as can be seen from Figure 3.11.

Finally in Figure 3.12 the comparison between the traditional lump mass described method and Biot method is demonstrated. The significant difference between the methods can be interpreted as a justification of this work.

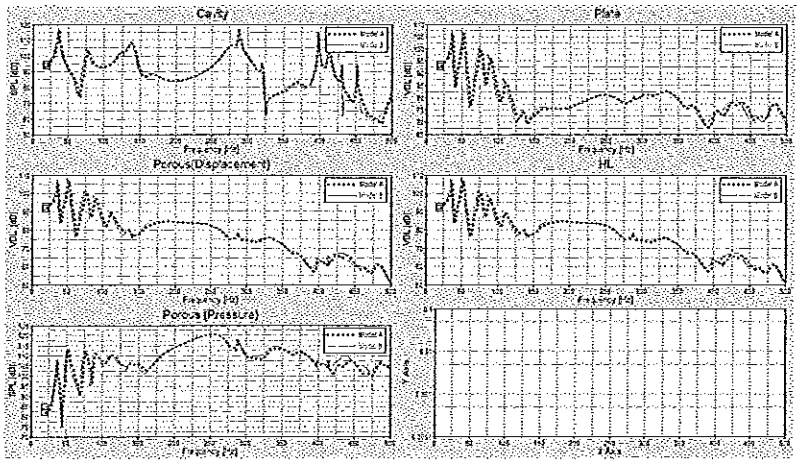

Figure 3.6: Comparison between Models A & B

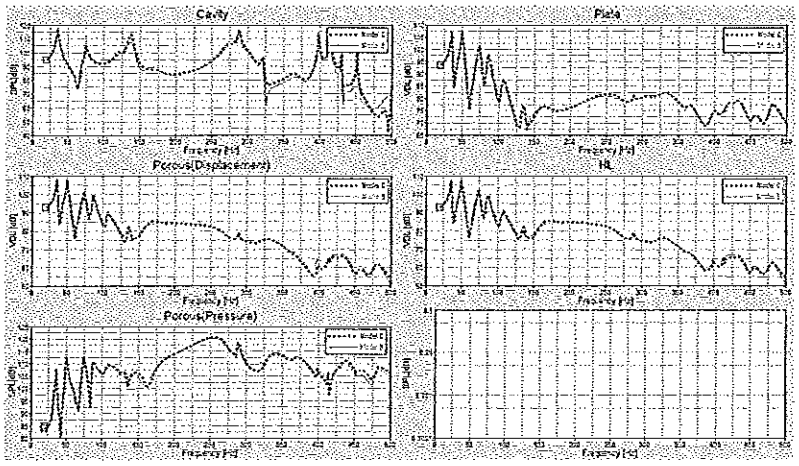

Figure 3.7: Comparison between Models B & C

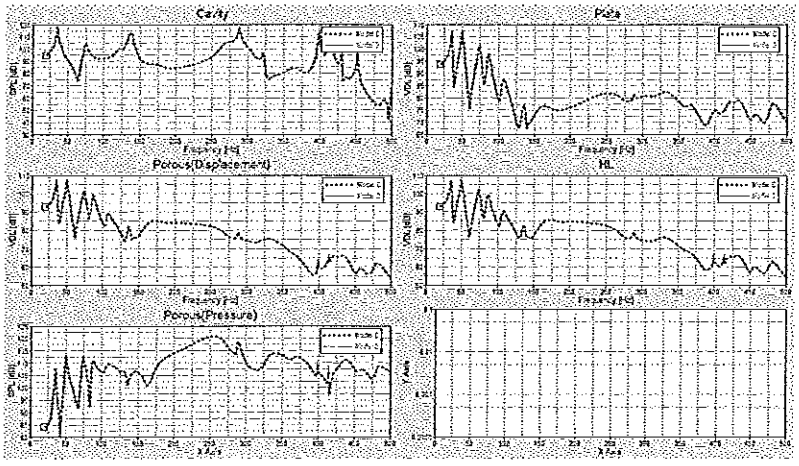

Figure 3.8: Comparison between Models C & D

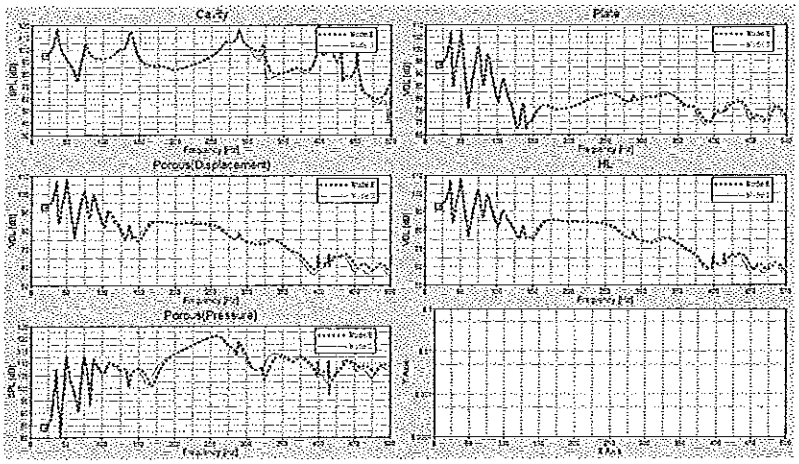

Figure 3.9: Comparison between Models D & E

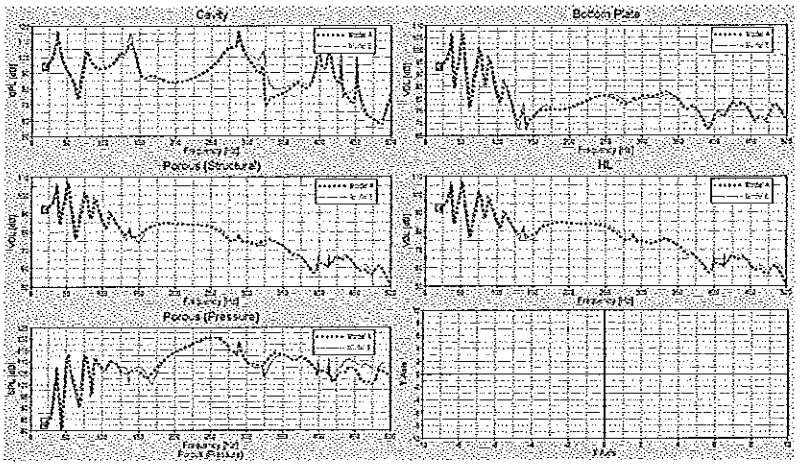

Figure 3.10: Comparison between Models A & E

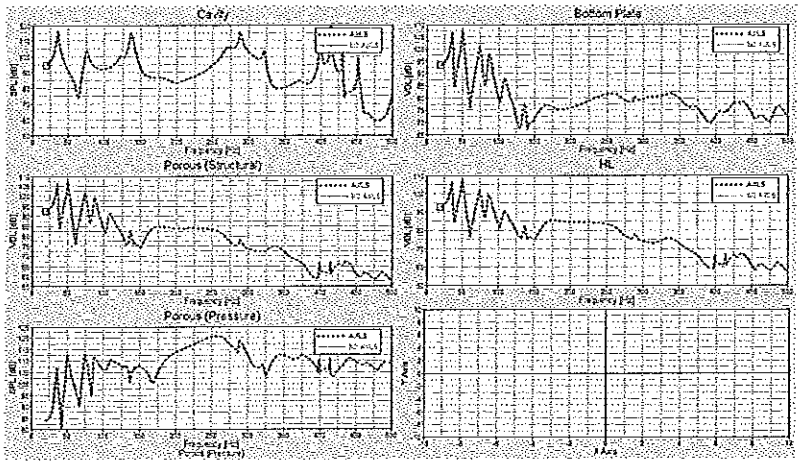

Figure 3.11: Model E with and without AMLS

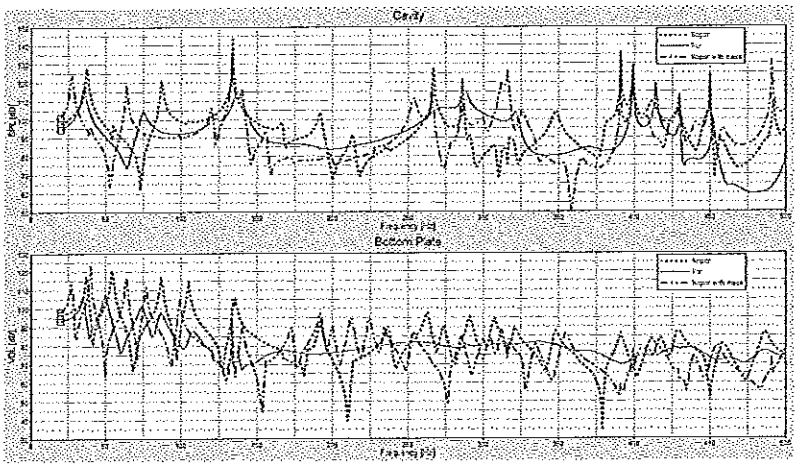

Figure 3.12: Porous, bare steel plate and distributed mass

3.4 Conclusion

By manipulating various finite element parameters like element type and connection type as well as using a multi-level substructuring tool; the possible effects on the results tried to be revealed. The differences that has been occurred during the process of transforming an academic finite element model to a more industrial standard are considered to be in an acceptable range. The most significant difference occurred at the very first step namely changing solid element type of the steel base plate into shell element type. This difference could be studied further by increasing the layer of solid elements and observe the convergence direction. In this manner the results of the model with solid elements would converge better to the linear elastic model. Thus one could comment on how far the shell elements in this case can represent the reality.

Chapter 4

Implementation on Body-in-Blue

Next and the final step of the project is forming the finite element models of the real insulation out of CAD data make necessary adjustments in the mesh and finally include the poroleastic EXEL calculations into the elastic NASTRAN body-in-blue calculations. Altough using EXEL with NASTRAN is straight forward there are a lot of potholes while using this software with different versions of NASTRAN and with additional softwares like AMLS. These will be discussed in the Discussion part in detail later on.

4.1 Preparation for FE calculations

The carpet CADs at hand were rough drawings which had not been built for the dynamic calculation purposes. In figure 4.1 there is the overlook of the carpets.

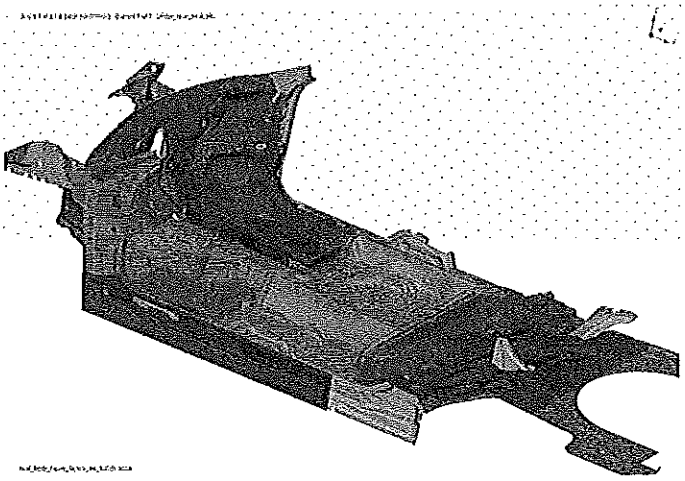

Figure 4.1: Overlook

There are 7 pieces of carpets (Figures 4.2 and 4.3) which are:

- Firewall Insulation
- Right and Left Front Floor Carpets (2 pieces)
- Tunnel Insulation
- Right and Left Rear Floor Carpets (2 pieces)

- Rear Underseat Carpet

All the pieces consist of two layers of different material. The bottom layers of all carpets made of foam. The top layer on the dashboard has an heavy layer others have AFR (Air Flow Resistant) layers. This is essential since the coupling between top layers of the insulation and the cavity differs between heavy layers and AFR layers. More details can be found on section 4.2.

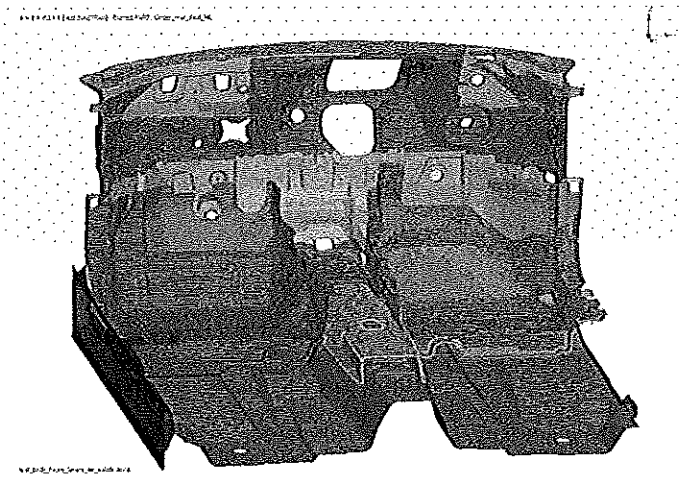

Figure 4.2: Dash-Tunnel Insulation and Front Carpets

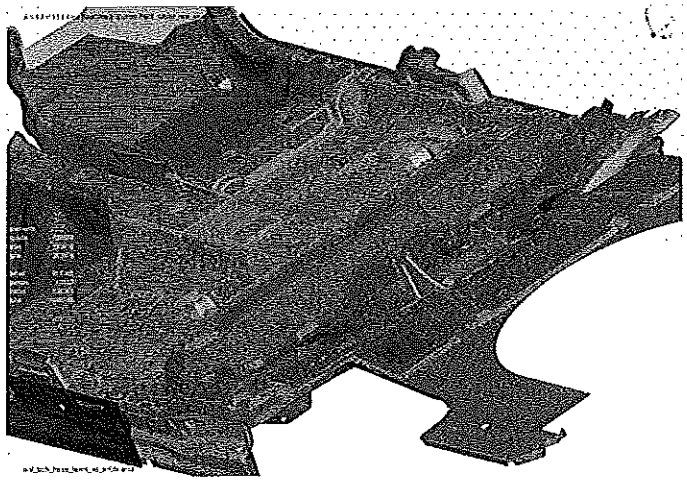

Figure 4.3: Front and Rear Floor Carpets

4.2 On the Coupling

The most challenging task of all in this modelling process was the coupling. Since the complexity of the geometry and inconsistencies between the mesh sizes and types node-to-node RBE2 coupling was impossible to apply. Instead, connections had to be automatically generated by another software from CDH called CDH/CONNECT. The software is capable of connecting irregular geometries and creating RBE3s for elastic to poroelastic coupling (eg. steel to foam),

RBE3s for poroelastic to poroelastic coupling (eg. foam to AFR)and MPCs for fluid to poroelastic coupling (eg. AFR to cavity). However there is a little detail on this type of connection. According CDH/EXEL manual:

- The pressure DOFs of the acoustic media are "connected" to the structural DOFs of the porous material via the standard NASTRAN "area matrix" (ACMODL). As in the standard structure-acoustic analysis, the acoustic mesh and the porous mesh do not have to be the coincident.
- In addition, the pressure DOF of the acoustic media (DOF 1) must be connected to the pressure DOF in the porous material media (DOF 4).

This is due to EXEL considers the 4th rotational DOF of solid element poroelastic material as the pressure DOF inside the structure. That is why it needs to be exclusively coupled the 1st pressure DOF of the cavity. If the coupling connections would be summarized:

- RBE3 for $DOF\,123 \rightarrow 123$ (Poroelastic to Elastic)
- RBE3 for $DOF\,1234 \rightarrow 1234$ (Poroelastic to Poroelastic)
- MPC for $DOF\,4 \rightarrow 1$ (Poroelastic to Cavity)

4.3 Results

Unfortunately due to time limitations and software issues whole full BIB with all carpets could not be run. The extreme need for CPU time as well as some bugs (might be due to the carpet models at hand as they are meshed in haste) in the software prevented the final results to be produced. However the dash insulation had been run successfully and the NTF results are presented on Figure 4.4.

Dash Carpet-Coarse Mesh	Modes (Structure)	Modes (Cavity)	FRF	Total
Elastic with AMLS	1 h 21 min	3 min	32 min	$\approx 2h$
EXEL with AMLS	1 h 21 min	3 min	83 h	$\approx 84h$
EXEL without AMLS	57 h	3 min	83 h	$\approx 140h$

Table 4.1: Runtimes Comparison

On the figure the traditional approach for including poroelastic materials into the model namely elastic approximation for poroelastic materials as smeared mass and the Biot approach incorporated by CDH/EXEL is compared. According to the figure the difference starts to appear towards mid frequency range after 200 Hz.

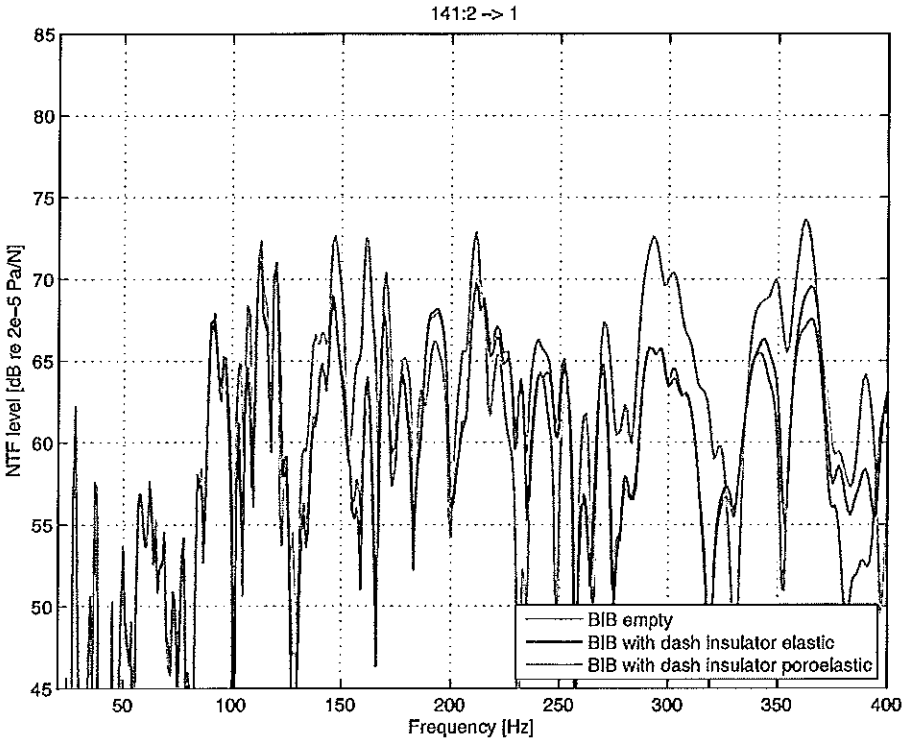

Figure 4.4: Elastic vs. Poroelastic Solution

4.4 Conclusion

The implementation of advanced modelling and FE calculations of poroelastic carpets into the industrial routines was aimed however the final goal was not achieved due to financial, time and administrative limitations. However important findings were revealed during the implementation process and most of them identified and solved especially related to coupling issues. Next step would be to complete this study with all carpets and try to optimize the time and resource spent also compare the results with actual measurement results to determine the accuracy.

Bibliography

[CDH, 2011] (2011). http://www.cdh-ag.com/de/exel.html/.

[Allard and Atalla, 2009] Allard, J. and Atalla, N. (2009). *Propagation of sound in porous media: modelling sound absorbing materials.* Wiley.

[Atalla et al., 1998] Atalla, N., Panneton, R., and Debergue, P. (1998). A mixed displacement-pressure formulation for poroelastic materials. *The Journal of the Acoustical Society of America*, 104:1444.

[Biot and Willis, 1957] Biot, M. and Willis, D. (1957). The elastic coefficients of the theory of consolidation. *J. appl. Mech*, 24(4):594–601.

[Champoux and Allard, 2009] Champoux, Y. and Allard, J. (2009). Dynamic tortuosity and bulk modulus in air-saturated porous media. *Journal of Applied Physics*, 70(4):1975–1979.

[Johnson et al., 1987] Johnson, D., Koplik, J., and Dashen, R. (1987). Theory of dynamic permeability and tortuosity in fluid-saturated porous media. *Journal of Fluid Mechanics*, 176:379–402.

[Johnson et al., 1986] Johnson, D., Koplik, J., and Schwartz, L. (1986). New pore-size parameter characterizing transport in porous media. *Physical review letters*, 57(20):2564–2567.